Development of a High Speed PM Brushless DC Motor for Driving Embroidery Machines

Jiaxin Chen, Youguang Guo, *Senior Member, IEEE*, and Jianguo Zhu, *Senior Member, IEEE*

***Abstract*—This paper presents the development of a permanent magnet (PM) brushless DC motor for driving high speed embroidery machines by employing advanced design and analysis techniques. In the design of the motor, magnetic field finite element analyses are conducted to accurately calculate the key motor parameters such as the air gap flux, back electromotive force (*emf*), and inductance, etc. Based on the numerical magnetic field solutions, a modified incremental energy method is introduced to effectively calculate the self and mutual inductances of the stator windings. A phasor diagram is derived to compute the motor's steady state characteristics. To predict the dynamic performance and increase the prediction accuracy, a Simulink-based model is built to simulate the motor performance with the real waveforms of applied phase voltage, back *emf* and current. The motor prototype has been constructed and tested with both a dynamometer and a high speed embroidery machine, which validates successfully the theoretical calculations.**

***Index Terms*—High speed motor, brushless DC motor, magnetic field finite element analysis, incremental inductance, performance simulation.**

I. Introduction

HIGH SPEED permanent magnet (PM) motors with brushless direct current (BLDC) control scheme have found wide applications in industrial and domestic appliance drive market in the past few decades, thanks to their advantages such as high efficiency, high power density and high drive performance [1-3]. Among the many applications are hard disk drives [4, 5], automotive fuel pumps [6], turbo-compressors [7], embroidery machines [8] and etc. The rapid development of BLDC motor drives has been in line with the advancement of PM materials, power switching devices, and control techniques [2]. To further improve the performance of BLDC drives, recent efforts have also been paid to the motor design and analysis by applying numerical techniques for accurate parameter prediction [9, 10], phase variable model including the effect of parameter variation [11, 12], performance simulation considering the real waveforms of back electromotive force (*emf*) [13], etc.

In this paper, a PM brushless DC motor is developed for driving high speed embroidery machines by employing various advanced techniques. In order to accurately compute the key motor parameters such as the air gap flux, back *emf*, and inductance, magnetic field finite element analyses (FEAs) are carried out. Based on the numerical magnetic field distribution, a modified incremental energy method is applied to effectively calculate the self and mutual inductances of the stator windings [14, 15].

To predict the motor performance, a phasor diagram with the sinusoidal waveforms (e.g. the fundamental components) of the applied phase voltage, back *emf* and current is derived under the optimum BLDC control condition. However, this method cannot predict the dynamic performance and the calculated steady-state characteristic is only an approximate as the harmonics are not taken into account. Therefore, a Simulink-based simulation model is also built to simulate the motor performance with the real waveforms of the applied phase voltage, back *emf* and current.

The rise rate of armature current is limited by the winding inductances, and this may affect the output performance of the motor, especially when operating at high speed. Therefore, it is necessary to investigate whether or not the motor can reach the required electromagnetic torque and speed at a given voltage. This is studied by the proposed simulation model.

The developed motor prototype has been fabricated and tested with both a dynamometer and a high speed embroidery machine. Theoretical calculations are validated by the good agreement with the experimental results.

II. Motor Configuration and Major Dimensions

Fig. 1 illustrates the magnetically relevant parts of the motor prototype. The laminated stator has 12 slots, in which the three phase single-layer windings are placed. The rotor core and shaft are made of solid mild steel, and four pieces of NdFeB PMs are mounted and bound on the surface of the rotor. The stator core has an inner diameter of 38 mm, outer diameter of 76 mm, and axial length of 38 mm. The main air gap length and the height of PMs along the radial magnetization direction are chosen as 1 mm and 2.5 mm, respectively. The motor is designed to deliver an output torque of 1.0 Nm at a speed of not less than 5000 rev/min.

Manuscript received May 26, 2006, revised May 15, 2007.

J. X. Chen is with the College of Electromechanical Engineering, Donghua University, Shanghai, 200051, China (email: chjiaxin@dhu.edu.cn).

Y. G. Guo and J. G. Zhu are with the Faculty of Engineering, University of Technology, Sydney, PO Box 123, Broadway, NSW 2007, Australia (e-mail: youguang@eng.uts.edu.au, joe@eng.uts.edu.au).

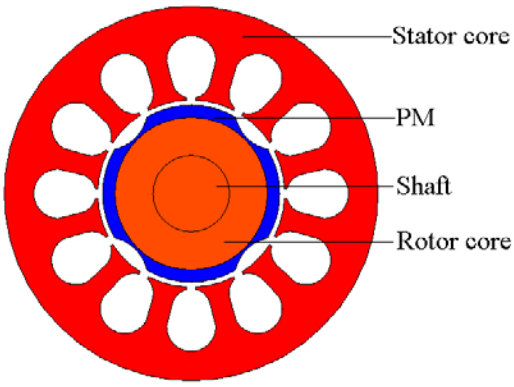

Fig. 1. Cross section of a PM brushless DC motor

III. Computation of Parameters and Performance

A. Winding Flux, Back emf and Cogging Torque

Magnetic field FEA can take into account the detailed structure and dimensions of the motor and the non-linearity of ferromagnetic materials, and hence can accurately compute the motor parameters and performance [9]. Fig. 2 illustrates the magnetic field distribution at no-load at the rotor position shown in Fig. 1, from which the phase winding flux produced by the rotor PMs, back *emf*, and cogging torque can be determined. The curves of these parameters against the rotor angular position or time can be obtained by a series of magnetic field FEAs at different rotor positions. Fig. 3 shows the no-load flux linking a coil (two coils form a phase winding) at different rotor positions. By the discrete Fourier transform, the magnitude of the fundamental of the coil flux was calculated as ϕ_1=0.543 mWb, and the *emf* constant can then be determined as 0.2457 Vs/rad, by

$$K_E = \frac{p}{2} N_s \frac{\phi_1}{\sqrt{2}} \tag{1}$$

where p=4 is the number of poles and N_s=320 the number of turns of a phase winding. The torque constant can be obtained by K_T=mK_E, where m=3 is the number of phases.

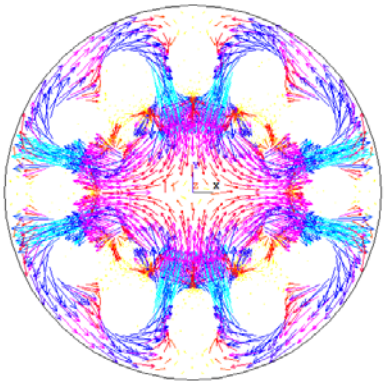

Fig. 2. Plot of no-load magnetic flux density vectors

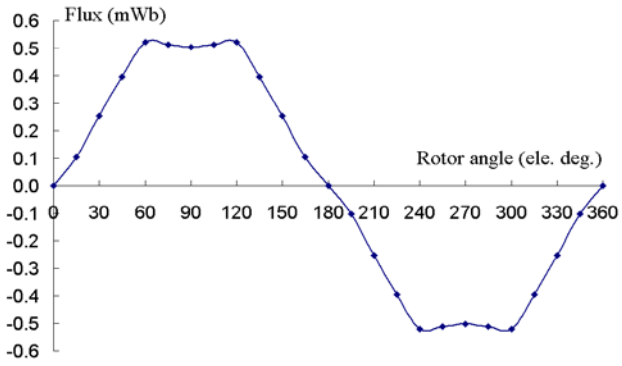

Fig. 3. Flux linking a coil versus rotor angle due to rotor PMs

From the no-load magnetic field distribution, the cogging torque curve can also be calculated by the Maxwell stress tensor method, or the virtual work method. It was found that the cogging torque of this surface-mounted PM motor is very small with a maximum value of 0.014 Nm.

B. Winding Inductance

The behavior of the motor equivalent electrical circuit is dominated by the incremental inductances rather than the apparent ones [16]. In this paper, the winding incremental inductances are calculated by a modified incremental energy method [14, 15], which includes the following steps: (1) For a given rotor position θ, conduct a non-linear field analysis considering the saturation due to the PMs to find the operating point of the motor, and save the incremental permeability in each element; (2) Set the remanence of PMs to be zero, and conduct linear field analyses with the saved permeabilities under perturbed stator current excitations, i.e. assigning the 3 phase winding currents as (i_a,i_b,i_c) = $(\Delta i,\Delta i,0)$, $(\Delta i,0,\Delta i)$, $(0,\Delta i,\Delta i)$, $(\Delta i,0,0)$, $(0,0,\Delta i)$, and $(0,\Delta i,0)$, respectively; (3) Calculate the co-energy for each current excitation; and (4) Calculate the incremental inductances by

$$L_{aa}(\theta) = L_{bb}(\theta) = L_{cc}(\theta) = \frac{2W_c(\Delta i,0,0,\theta)}{(\Delta i)^2} \tag{2a}$$

$$L_{ab}(\theta) = L_{ba}(\theta) = \frac{W_c(\Delta i,\Delta i,0,\theta) - W_c(0,\Delta i,0,\theta) - W_c(\Delta i,0,0,\theta)}{(\Delta i)^2} \tag{2b}$$

$$L_{bc}(\theta) = L_{cb}(\theta) = \frac{W_c(0,\Delta i,\Delta i,\theta) - W_c(0,\Delta i,0,\theta) - W_c(0,0,\Delta i,\theta)}{(\Delta i)^2} \tag{2c}$$

$$L_{ca}(\theta) = L_{ac}(\theta) = \frac{W_c(\Delta i,0,\Delta i,\theta) - W_c(0,0,\Delta i,\theta) - W_c(\Delta i,0,0,\theta)}{(\Delta i)^2} \tag{2d}$$

Fig. 4 shows the calculated self and mutual incremental inductances at different rotor positions.

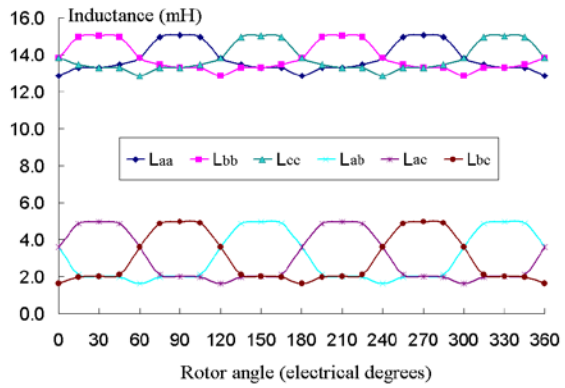

Fig. 4. Winding inductances versus rotor angle

C. Calculation of Steady State Characteristics

To predict the motor's steady state characteristics with the optimum BLDC scheme, a phasor diagram is derived as shown in Fig. 5, where E_1 is the back *emf*, R_1 stator winding resistance, L_1 synchronous inductance which equals the self inductance plus half of the mutual inductance, V_1 the rms values of the stator phase voltage, I_1 the phase current, and ω the angular frequency.

For simplicity, the winding inductances can be considered as constants, e.g. the average values. From Fig. 4, the average self-inductance of a phase winding is L=13.8 mH, and the average mutual inductance between two phase windings is M=3.0 mH.

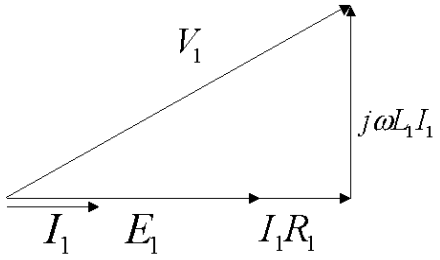

Fig. 5. Phasor diagram when the motor is in optimum BLDC condition

The motor is assumed to operate in the optimum brushless DC mode, i.e. I_1 in phase with E_1, so that the electromagnetic torque can be obtained by

$$T_{em} = \frac{mE_1 I_1}{\omega_r} \tag{3}$$

where ω_r is the rotor speed in rad/s. The rms value of the back *emf* is determined by $E_1=k_E\omega_r$. For a given terminal voltage, V_1, the torque/speed curve can be derived as

$$\omega_r = \frac{\sqrt{\left(\frac{R_1 T_{em}}{m}\right)^2 + \left[\left(\frac{P}{2}L_1\frac{T_{em}}{K_T}\right)^2 + K_E^2\right]\left[V_1^2 - \left(\frac{R_1 T_{em}}{K_T}\right)^2\right]} - \frac{R_1 T_{em}}{m}}{\left(\frac{P}{2}L_1\frac{T_{em}}{K_T}\right)^2 + K_E^2} \tag{4}$$

Fig. 6 illustrates the torque/speed curves with different values of terminal voltage.

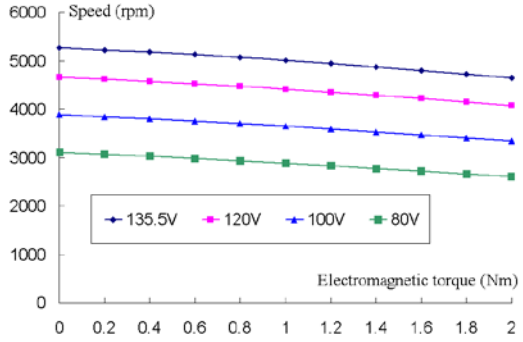

Fig. 6. Torque/speed curves at different phase voltages

IV. Performance Simulation

In Section III, the motor's steady state characteristics were predicted based on sinusoidal flux, back *emf*, and current. In this section, the motor performance is also studied with the square wave voltages and trapezoidal wave *emfs* by a Matlab/Simulink-based model. This study aims to investigate the dynamic performance, e.g. whether or not the motor can reach the specified speed with the rated load at a given voltage since the motor output can be limited by the winding inductance, especially at high speed operation.

A. Modeling of the Brushless DC Motor with Square Waveform Voltage

The voltage equations of the three phase windings can be written as

$$\begin{bmatrix} V_A \\ V_B \\ V_C \end{bmatrix} = \begin{bmatrix} R_1 & 0 & 0 \\ 0 & R_1 & 0 \\ 0 & 0 & R_1 \end{bmatrix}\begin{bmatrix} i_a \\ i_b \\ i_c \end{bmatrix} + \begin{bmatrix} L & M & M \\ M & L & M \\ M & M & L \end{bmatrix}\frac{d}{dt}\begin{bmatrix} i_a \\ i_b \\ i_c \end{bmatrix} + \begin{bmatrix} E_a \\ E_b \\ E_c \end{bmatrix} \tag{5}$$

where V_a, V_b, and V_c are the phase voltages, i_a, i_b, and i_c the phase currents, and E_a, E_b, and E_c the phase back *emfs*. For the symmetrically distributed star connected three phase windings, the phase currents obey

$$i_a + i_b + i_c = 0 \tag{6}$$

For the motor operating with square waveform voltages, the conduction region of phase current corresponds to the peak value segment of the back *emf*, E_m.

The electromagnetic torque is calculated by

$$T_{em} = \frac{E_a i_a + E_b i_b + E_c i_c}{\omega_r} \tag{7}$$

The motion equation is

$$\frac{d\omega_r}{dt} = \frac{T_{em} - T_L - \delta_0\omega_r}{J} \tag{8}$$

where T_L is the load, δ_0 the friction coefficient, and J the total inertia of the rotating parts.

B. Simulink-based Simulation of the Motor Drive System

According to (5)-(8), a Simulink-based model, as shown in Fig. 7, is built for the brushless DC motor.

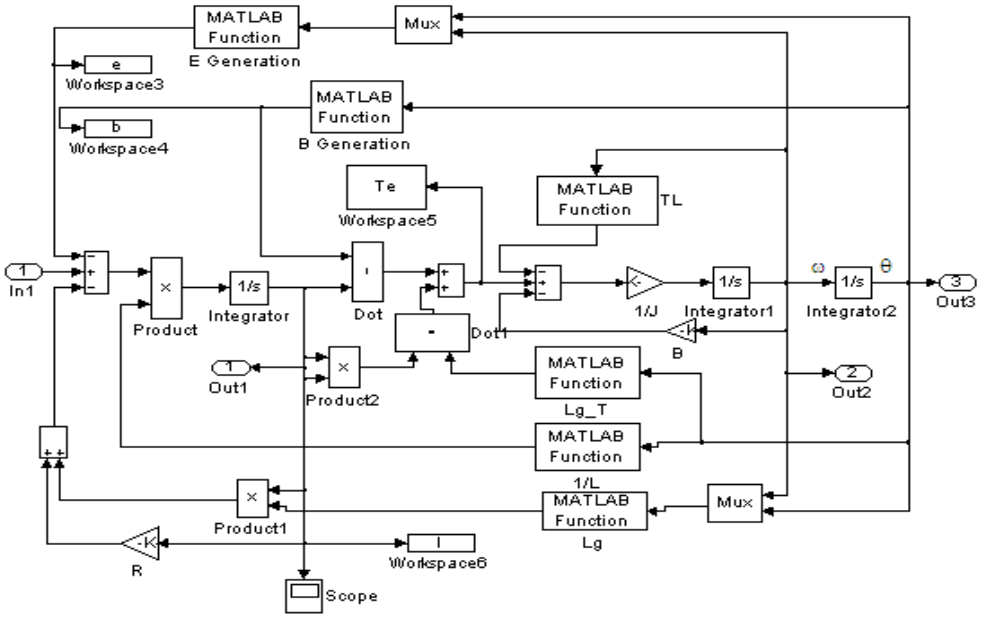

Fig. 7. Simulink-based model of the BLDC motor

The basic design requirement for the motor drive system is that for an output torque of 1.0 Nm, the steady-state speed should be no less than 5000 rpm when the inverter DC bus voltage is V_{dc}=310 VDC. By using the proposed model, the motor drive system is simulated under these conditions and some of the results are plotted in Figs. 8-13, showing that the motor can meet the design requirements.

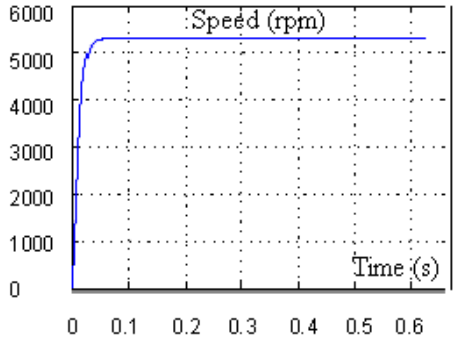

Fig. 8. Start-up speed curve with a load of 1.0 Nm when V_{dc}=310 V DC

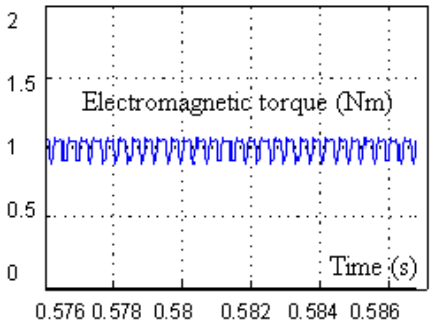

Fig. 9. Steady-state torque when V_{dc}=310 V DC

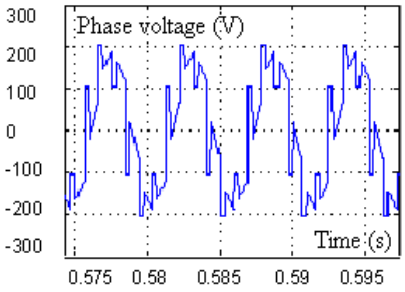

Fig. 10. Voltage of phase *a*

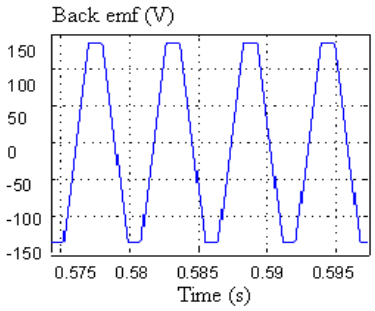

Fig. 11. Back *emf* of phase *a*

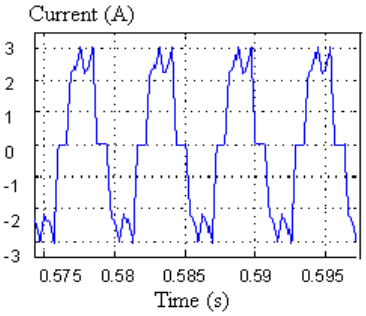

Fig. 12. Current in phase *a*

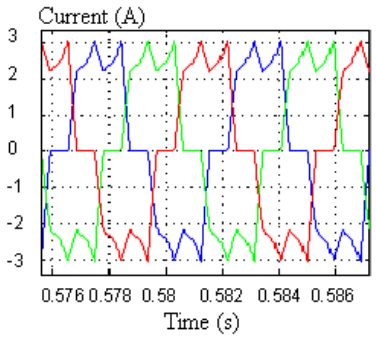

Fig. 13. Currents in three phase windings

V. Experimental Validation

The designed motor has been fabricated and successfully operated with a brushless DC control scheme. Experiments have been conducted on the prototype. The back *emf*, for example, was measured at different rotor speeds and the experimentally determined *emf* constant is 0.2464 Vs/rad, which is very close to the theoretical value. Fig. 14 shows the measured *emf* waveform, obtained by recording the open-circuit terminal voltage when the motor is driven at a certain speed. It can be seen that the *emf* waveform is similar to that of the computed flux in Fig. 3.

Fig. 15 shows the measured phase current, which agrees with the simulation (Fig. 11) in both waveform and magnitude. The steady-state mechanic characteristic is also measured as shown in Fig. 16. The speed has been normalized with the base of 6000 rpm. It can be found the motor can operate in a steady speed of more than 5000 rpm with the rated torque of 1.0 Nm when the input voltage is 220 VAC (310 VDC). The corresponding efficiency curve is also plotted in the figure.

Other parameters, such as the inductances are also in substantially agreement with the calculations.

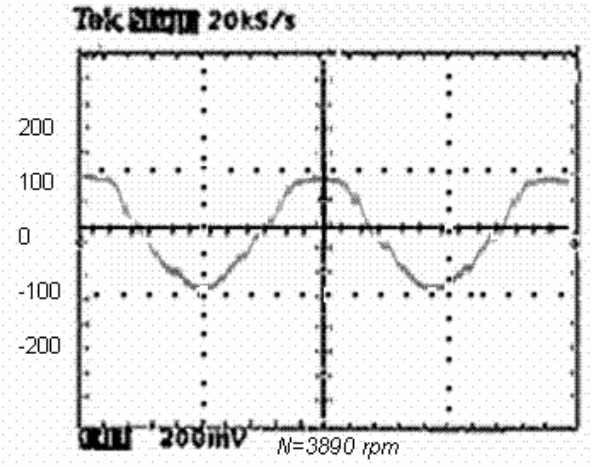

Fig. 14. Measured back *emf* waveform

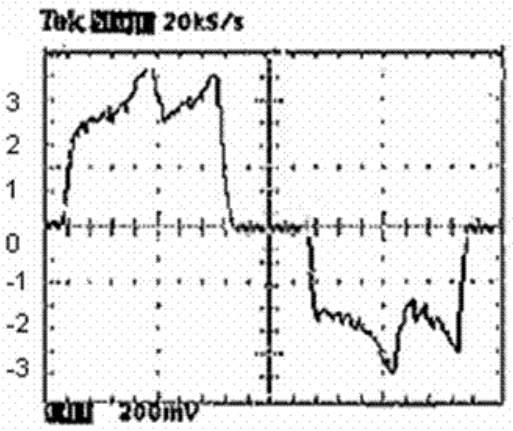

Fig. 15. Measured phase current

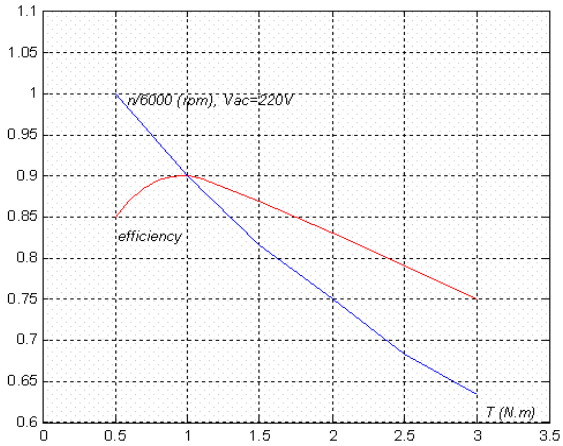

Fig. 16. Measured steady-state mechanical characteristic and efficiency

VI. Conclusion

This paper reports the design and analysis of a permanent magnet motor for driving high speed embroidery machines. The motor is operated by a brushless DC drive scheme. The motor performance is investigated with the fundamental components of the applied phase voltage, back *emf* and current by a phasor diagram, and with the real voltage, back *emf* and current waveforms by a Simulink-based simulation model.

For accurate computation of the motor parameters, the finite element magnetic field analysis is performed and improved formulations, e.g. the modified incremental energy method for calculating the self and mutual winding inductances, are used.

The motor has been constructed and tested with a brushless DC control scheme, validating the theoretical design and analysis.

References

[1] T. Kenjo, Permanent Magnet and Brushless DC Motors, *Oxford University Press*, 1985.

[2] T. S. Low, M. A. Jabbar, and M. A. Rahman, "Permanent-magnet motors for brushless operation," *IEEE Trans. Industry Applications*, Vol. 26, No. 1, Jan./Feb. 1990, pp. 124-129.

[3] N. Bianchi, S. Bolognani, and F. Luise, "High speed drive using a slotless PM motor," in *Proc. 35th Annual IEEE Power Electronics Specialist Conf.*, Aachen, Germany, 2004, pp. 458-463.

[4] G. Jang and M. G. Kim, "A bipolar-starting and unipolar-running method to drive a hard disk drive spindle motor at high speed with large

starting torque," *IEEE Tran. Magn.*, Vol. 41, No. 2, Feb. 2005, pp. 750-755.

[5] Q. Jiang, C. Bi, and A. A. Mamun, "An effective approach to predict performance of high speed BLDC motors in hard disk drives," in *Proc. 29th Annual Conf. of IEEE Industrial Electronics Society*, Nov. 2-6, 2003, pp. 2120-2125.

[6] J. Shao, D. Nolan, M. Teissier, and D. Swanson, "A novel microcontroller-based sensorless brushless DC (BLDC) motor drive for automotive fuel pumps," *IEEE Trans. Industry Applications*, Vol. 39, No. 6, Nov./Dec. 2003, pp. 1734-1740.

[7] S. M. Jang, H. W. Cho, J. Y. Choi, J. H. Park, and S. K. Choi, "Development of high-speed brushless DC motor for turbo-compressor," in *Proc. 8th Int. Conf. on Electrical Machines and Systems*, Nanjing, China, Sept. 27-29, 2005, pp. 877-882.

[8] T. W. Chun, J. R. Ahn, H. H. Lee, H. G. Kim, and E. C. Nho, "Development of servo motor drive systems for embroidery machines," in *Proc. 8th Russian-Korean Int. Symposium on Sci. and Tech.*, June 26 - July 3, 2004, pp. 310-314.

[9] Y. G. Guo, J. G. Zhu, P. A. Watterson, and W. Wu, "Development of a permanent magnet transverse flux motor with soft magnetic composite core," *IEEE Trans. Energy Conversion*, Vol. 21, No. 2, pp. 426-434, June 2006.

[10] Y. G. Guo, J. G. Zhu, J. X. Chen, and J. X. Jin, "Performance analysis of a permanent magnet claw pole SMC motor with brushless DC control scheme," in *Proc. Int. Power Electronics and Motion Control Conf.*, Shanghai, China, Aug. 13-16, 2006.

[11] O. A. Mohammed, S. Liu, and Z. Liu, "A phase variable model of brushless dc motors based on finite element analysis and its coupling with external circuits," *IEEE Tran. Magn.*, Vol. 41, No. 5, May 2005, pp. 1576-1579.

[12] O. A. Mohammed, S. Liu, and Z. Liu, "Physical modeling of PM synchronous motors for integrated coupling with machine drives," *IEEE Trans. Magn.*, Vol. 41, No. 5, May 2005, pp. 1628-1631.

[13] Y. S. Jeon, H. S. Mok, G. H. Choe, D. K. Kim, and J. S. Ryu, "A new simulation of BLDC motor with real back EMF waveform," in *Proc. 7th Workshop on Computers in Power Electronics*, Blacksburg, VA, July 16-18, 2000, pp. 217-220.

[14] Y. G. Guo, J. G. Zhu, H. W. Lu, R. Chandru, S. H. Wang, and J. X. Jin, "Determination of winding inductance in a claw pole permanent magnet motor with soft magnetic composite core," in *Proc. Australasian Universities Power Eng. Conf.*, Hobart, Australia, Sept. 25-28, 2005, pp. 491-496.

[15] Y. G. Guo, J. G. Zhu, and H. Y. Lu, "Accurate determination of parameters of a claw pole motor with SMC stator core by finite element magnetic field analysis," *IEE Proceedings - Electric Power Application*, Vol. 153, No. 4, July 2006, pp. 568-574.

[16] M. Gyimesi and D. Ostergaard, "Inductance computation by incremental finite element analysis," *IEEE Trans. Magn.*, Vol. 35, No. 3, pp. 1119-1122, May 1999.